NANO LETTERS
Letter
Cite This: Nano Lett. 2019, 19, 4627−4633
pubs.acs.org/NanoLett

Dimensional Crossover and Topological Nature of the Thin Films of a Three-Dimensional Topological Insulator by Band Gap Engineering

Zhenyu Wang,[*,†,‡,#] Tong Zhou,[†] Tian Jiang,[†,⊥] Hongyi Sun,[∥,○] Yunyi Zang,[§] Yan Gong,[§] Jianghua Zhang,[§,#] Mingyu Tong,[⊥] Xiangnan Xie,[†] Qihang Liu,[*,∥,▽] Chaoyu Chen,[*,∥] Ke He,[§,#] and Qi-Kun Xue[§,#]

[†]State Key Laboratory of High Performance Computing, College of Computer, National University of Defense Technology, Changsha 410073, P. R. China

[‡]National Innovation Institute of Defense Technology, Academy of Military Sciences PLA China, Beijing 100010, P. R. China

[§]State Key Laboratory of Low Dimensional Quantum Physics, Department of Physics, Tsinghua University, Beijing 100084, P. R. China

[∥]Shenzhen Institute for Quantum Science and Engineering (SIQSE) and Department of Physics, Southern University of Science and Technology (SUSTech), Shenzhen 518055, P. R. China

[⊥]College of Advanced Interdisciplinary Studies, National University of Defense Technology, Changsha 410073, P. R. China

[#]Beijing Academy of Quantum Information Sciences, Beijing 100084, P. R. China

[▽]Center for Quantum Computing, Peng Cheng Laboratory, Shenzhen 518055, P. R. China

[○]School of Physics, Southeast University, Nanjing 211189, P. R. China

Supporting Information

ABSTRACT: Identification and control of topological phases in topological thin films offer great opportunities for fundamental research and the fabrication of topology-based devices. Here, combining molecular beam epitaxy, angle-resolved photoemission spectroscopy, and *ab initio* calculations, we investigate the electronic structure evolution in $(Bi_{1-x}In_x)_2Se_3$ films ($0 \le x \le 1$) with thickness from 2 to 13 quintuple layers. By employing both thickness and In substitution as two independent "knobs" to control the gap change, we identify the evolution between several topological phases, i.e., dimensional crossover from a three-dimensional topological insulator to its two-dimensional counterpart with gapped surface state, and topological phase transition from a topological insulator to a normal semiconductor with increasing In concentration. Furthermore, by introducing In substitution, we experimentally demonstrated the trivial topological nature of Bi_2Se_3 thin films (below 6 quintuple layers) as two-dimensional gapped systems, consistent with our theoretical calculations. Our results provide not only a comprehensive phase diagram of $(Bi_{1-x}In_x)_2Se_3$ and a route to control its phase evolution but also a practical way to experimentally determine the topological properties of a gapped compound by a topological phase transition and band gap engineering.

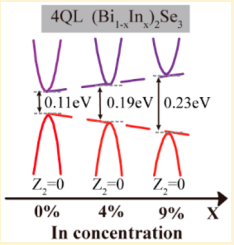

KEYWORDS: *Topological insulator, band engineering, topological phase transition, dimensional crossover, density functional theory, angle-resolved photoemission spectroscopy*

One of the central goals of modern condensed matter physics is to realize novel quantum phases of matter and develop practical control over their properties, holding promise for a new generation of photonic, electronic, and energy technologies. Topological insulators (TIs) are new phases of quantum matter with unique bulk band topology and surface states protected by certain symmetries.[1−3] For example, the strong TIs,[4] classified by a topological Z_2 invariant $\nu_0 = 1$, are protected by time-reversal symmetry and thus possess metallic surface states at the boundary to a trivial insulator[5,6] (e.g., band insulator or vacuum, $\nu_0 = 0$) with an odd number of Dirac cones. The discovery of the TIs has led to the prediction and realization of other new topological states including the topological crystalline insulator (TCI),[3] topological Kondo insulator,[7] topological Dirac/Weyl semimetal,[8] and so on. The emergence of such rich topological systems offers a fertile ground, for not only the exploration of exotic quantum phenomena such as the supersymmetry state,[9] interacting TIs,[10] Floquet topological insulator,[11] and so on, but also the realization of novel topology-based devices like topological transistors,[12] spin torque devices,[13] and topological photodetectors.[14]

For most of such applications, ultrathin films (few atomic layers thick) of three-dimensional (3D) TIs with a well-

Received: April 21, 2019
Revised: June 11, 2019
Published: June 12, 2019

DOI: 10.1021/acs.nanolett.9b01641
Nano Lett. 2019, 19, 4627−4633

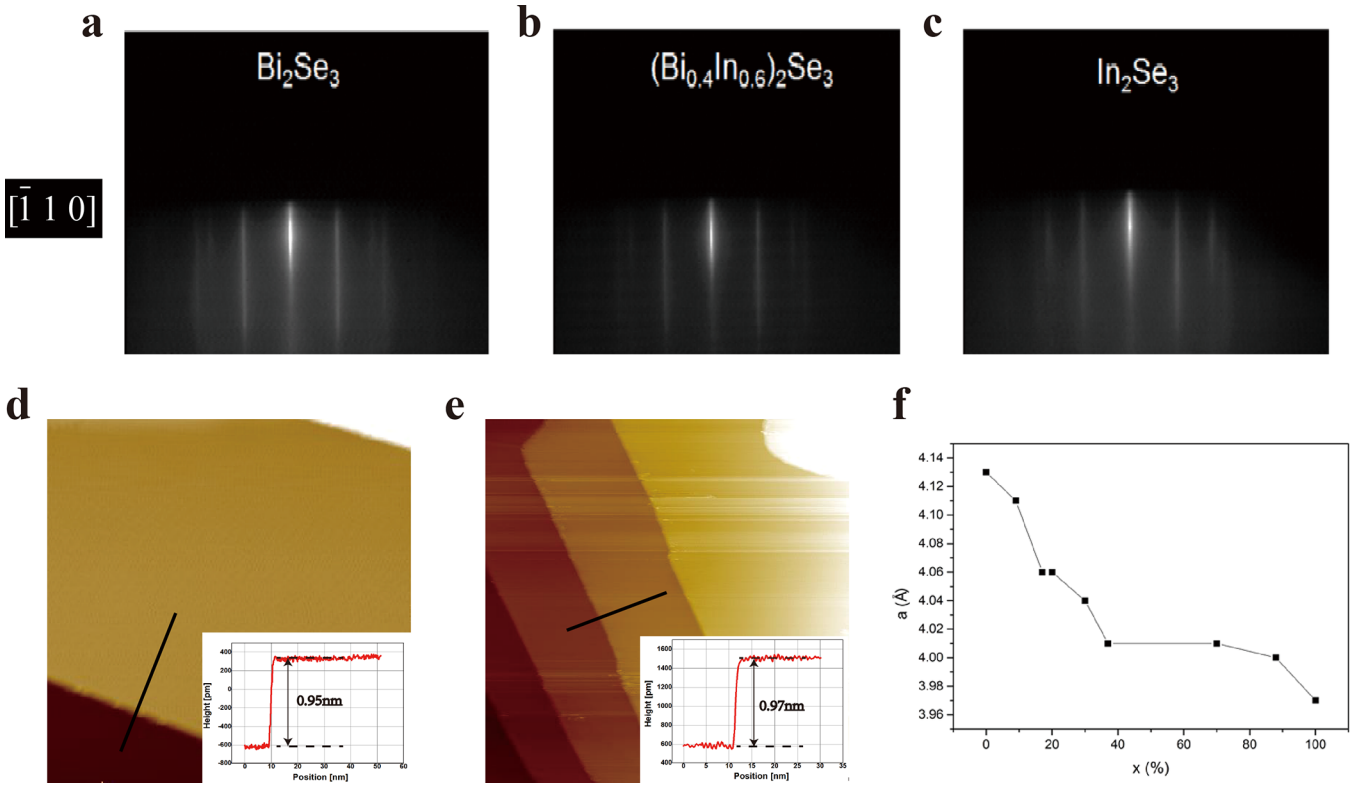

Figure 1. Characteristics of $(Bi_{1-x}In_x)_2Se_3$ thin films by RHEED and STM. (a–c) Bi_2Se_3, $(Bi_{0.4}In_{0.6})_2Se_3$, and In_2Se_3 RHEED patterns. (d) STM image of Bi_2Se_3 film (4 QLs, 65 nm × 65 nm) on graphene substrate. The inset shows the STM line profile along the black lines, which shows a 0.95 nm step corresponding to the height of 1 QL. (e) STM image of In_2Se_3 film (13 QLs, 100 nm × 100 nm) on graphene substrate. The inset also shows the corresponding line profile. (f) Substitution x-dependent lattice constant a of $(Bi_{1-x}In_x)_2Se_3(111)$ films.

controlled number of layers and composition are inevitably required. During the truncation along one direction, the hybridization between opposite surfaces opens a gap in the surface Dirac cone and drives the system into a phase with gapped surface states. For a typical 3D TI such as Bi_2Se_3, an interesting question thus arises: do the thin films with observable hybridization gap,[15] i.e., 1–5 quintuple layers (QLs, where 1 QL ≈ 1 nm), manifest two-dimensional (2D) quantum spin Hall insulators with an inverted band gap or not? It was theoretically predicted by a continuous Hamiltonian model and density functional theory (DFT) calculations that the topological feature of Bi_2Se_3 thin films exhibits an oscillatory manner with increasing thickness.[16,17] Nevertheless, angle-resolved photoemission spectroscopy (ARPES) measurements directly performed on Bi_2Se_3 thin films cannot tell the sign of the hybridization gap,[15] while transport experiments have to suffer the bulk conductivity because of the intrinsic n-type doping.[18,19] Therefore, no conclusive answer to the question has been drawn yet.

To understand the topological nature of a new quantum phase, a powerful approach is to study its evolution from an understood phase through phase transition. Topological phase transition (TPT) refers to transition from one topologically nontrivial phase to another or to a topologically trivial phase, and vice versa. The realization of TPT involves utilization of structural or compositional degrees of freedom as an external "knob", such as alloying a normal insulator (NI) with TI components or applying strain or electric field to an NI, attempting to induce thereby band inversion. For example, $BiTlSe_2$ bulk crystal doped with S, $BiTl(S_{1-x}Se_x)_2$, is the first system where TPT was observed.[20,21] TPT from topological-metallic to normal-insulating states has further been realized in $(Bi_{1-x}In_x)_2Se_3$[19,22–24] and $(Bi_{1-x}Sb_x)_2Se_3$[25] single crystals and films. To date, the experimental exploration of TPT has been mainly limited on thick films and bulk samples,[20–22,24–26] whereas only few thickness-dependent transport measurements have focused on ultrathin $(Bi_{1-x}In_x)_2Se_3$ films down to 2 QLs.[19,23] For ultrathin $(Bi_{1-x}In_x)_2Se_3$ samples, with increasing In substitution, the spin–orbit coupling (SOC) strength decreases and drives the system from a topologically nontrivial state to a trivial state, accompanied by the inverted bulk gap closure and reopening.[19,23] During such a process, hybridization comes into play due to the increase of the surface penetration depth with decreasing bulk gap size, manifesting itself as a dimensional crossover as the films change from being 3D to approximately 2D. For ultrathin TI films, this picture has been merely deduced from transport behaviors,[19,23] while it lacks direct and detailed band structure investigation [say, via ARPES]. Furthermore, the general picture of TPT in $(Bi_{1-x}In_x)_2Se_3$ still contains a controversial description of the band structure evolution concerning whether it is a linear gap-closure[19,22,23] or a sudden gap-closure scenario.[24]

In this work, we study the topology and TPT of ultrathin Bi_2Se_3 films by employing structural and compositional "knobs". Using molecular beam epitaxy (MBE) we have grown high-quality indium-doped Bi_2Se_3 films ($(Bi_{1-x}In_x)_2Se_3$), with thicknesses ranging from 2 to 13 QLs and In substitution x from 0 to 1. Systematic *in situ* ARPES measurements have been performed to monitor the evolution of both bulk and surface band structure. A dimension (thickness)-substitution phase diagram has been drawn. In this phase diagram, we have identified several different

DOI: 10.1021/acs.nanolett.9b01641
Nano Lett. 2019, 19, 4627–4633

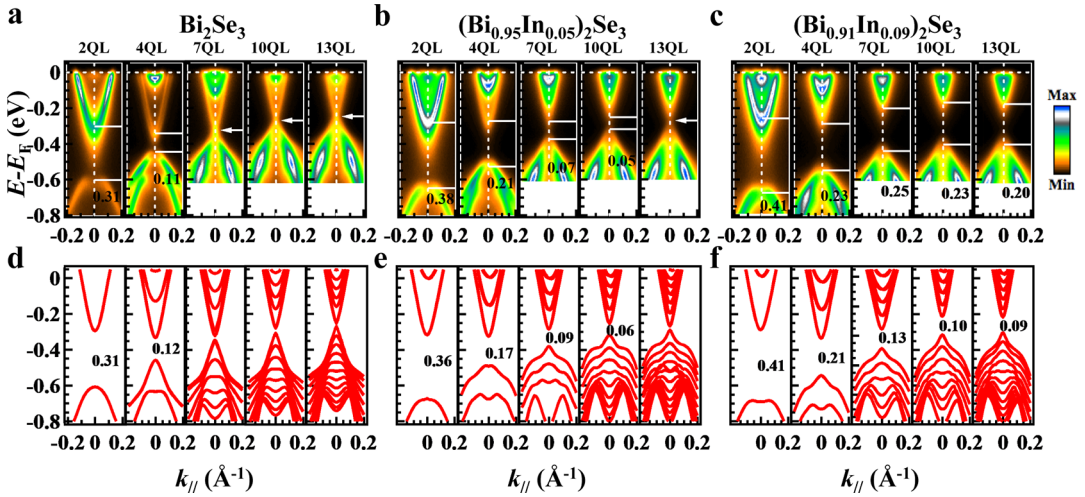

Figure 2. Band structure evolution of $(Bi_{1-x}In_x)_2Se_3$ thin films with increasing number of layers for different substitution level x. (a–c) ARPES-measured band structure for different In concentration x and number of layers. The white solid lines indicate the VBM and CBM positions. The corresponding estimated gap size (in eV) is also shown for each composition. Note the surface state gap in parts a and b and bulk state gap in part c. The white arrows indicate the position of the Dirac point. (d–f) Corresponding theoretically calculated band structure. The size of the band gap is also indicated.

quantum states, i.e., 3D TI with gapless surface states and its 2D counterpart hosting hybridization-induced gapped surface states (hereafter referred to as 2D GSS) below the critical substitution concentration ($x \leq 5\%$) and NI state ($9\% \leq x \leq 100\%$). The dimensional crossover from 3D TI to 2D GSS is driven by both SOC and surface state hybridization and thus can be manipulated through bulk band gap engineering by either thickness control or substitution control, while the transition from 3D TI or 2D GSS to NI is driven solely by SOC, independent of film thickness. More importantly, we illustrate that one can create a phase evolution process by introducing an external knob and monitoring the existence of TPT to determine the topological nature of the initial phase. Our ARPES-measured gap evolution of thin film $(Bi_{1-x}In_x)_2Se_3$ (e.g., 4 QLs) by tuning the amount of In alloying shows a monotonic increasing feature, indicating that, as 2D systems, the 2D GSS films, particularly Bi_2Se_3 ultrathin films with an observable hybridization gap (i.e., 1–5 QLs), are all topologically trivial. Such results are confirmed by our DFT-calculated Z_2 invariants by using a hybrid correlation-exchange functional. Compared with the previous work manipulating the band gap of Bi_2Se_3 thin films with the film thickness as the only "knob",[15] our findings provide a practical way to control the dimensional crossover of the topological phase evolution in $(Bi_{1-x}In_x)_2Se_3$ ultrathin films by composition alloying, which is critical for potential device applications. Furthermore, our work provides a unique approach to experimentally determine the topological nature of an insulating phase by monitoring the band gap evolution under the tuning of an external knob, such as SOC and tensile strain.

Results. *Growth and characterization of $(Bi_{1-x}In_x)_2Se_3$ thin films.* $(Bi_{1-x}In_x)_2Se_3$ films with variable thickness (2, 4, 7, 10, and 13 QLs) were grown by MBE on single-layer graphene, prepared by graphitizing a SiC substrate.[27] For each thickness, x varies from 0% to 100%. The Bi flux was calibrated by measuring the thickness of as-grown Bi_2Se_3 films using scanning tunneling microscopy (STM) and atomic force microscopy (AFM). Then, the Bi flux was fixed. The In flux was calibrated by measuring the thickness of as-grown In_2Se_3 films. In such a way the flux ratio of Bi and In was determined for each x of $(Bi_{1-x}In_x)_2Se_3$, and the corresponding films were grown by simultaneously depositing Bi, In, and Se atoms from independent sources. As-grown films were preliminarily characterized by reflection high-energy electron diffraction (RHEED) and STM. Figure 1a–c presents typical RHEED patterns of Bi_2Se_3, $(Bi_{0.4}In_{0.6})_2Se_3$, and In_2Se_3, from which the corresponding lattice constant can be calculated. For In_2Se_3, the hexagonal in-plane lattice constant (a) is calculated as $a \approx 3.97$ Å, consistent with the value of α-$In_2Se_3(111)$ reported in previous works.[28] For Bi_2Se_3, $a \approx 4.13$ Å, also in agreement with the previously reported value.[29] Figure 1f summarizes the evolution of a with increasing chemical composition ratio x in $(Bi_{1-x}In_x)_2Se_3$. It is clear that a decreases monotonically with increasing x, due to the fact that In atoms are smaller than Bi atoms. Figure 1d,e shows the STM images of as-grown Bi_2Se_3 and In_2Se_3, respectively. The height profile of the corresponding QLs can be extracted across the steps at the film edge, as shown in the insets. The QL thickness is about 0.95 nm for Bi_2Se_3 and 0.97 nm for In_2Se_3, consistent with previous works.[28] Furthermore, the sharp RHEED streaks and the atomically flat morphology demonstrate the high crystalline quality of the as-grown $(Bi_{1-x}In_x)_2Se_3$ films of variable thickness, which is suitable for further ARPES investigation.

Dimensional Crossover. Figure 2 and Figure S1 present the band evolution of $(Bi_{1-x}In_x)_2Se_3$ films with systematic substitution and layer number control. Generally speaking, for all the spectra, the Fermi level intersects the bulk conduction band due to the intrinsic doping from, e.g., Se vacancies. Nevertheless, we use terms like TI in the present work since we focus on the fundamental band structure rather than the transport properties that related to the position of chemical potential. We locate the position of the conduction band minimum (CBM) and valence band maximum (VBM) through energy-distribution curve (EDC) analysis (see Figures S2 and S3 for detail). The estimated gap size, i.e., the energy difference between the CBM and VBM, is shown for each substitution concentration in the corresponding panels. It is widely accepted that the surfaces of 3D TI host the gapless Dirac cone in bulk crystals and thick films, and this is exactly the case for Bi_2Se_3 films thicker than 6 QLs as shown in Figure

DOI: 10.1021/acs.nanolett.9b01641
Nano Lett. 2019, 19, 4627–4633

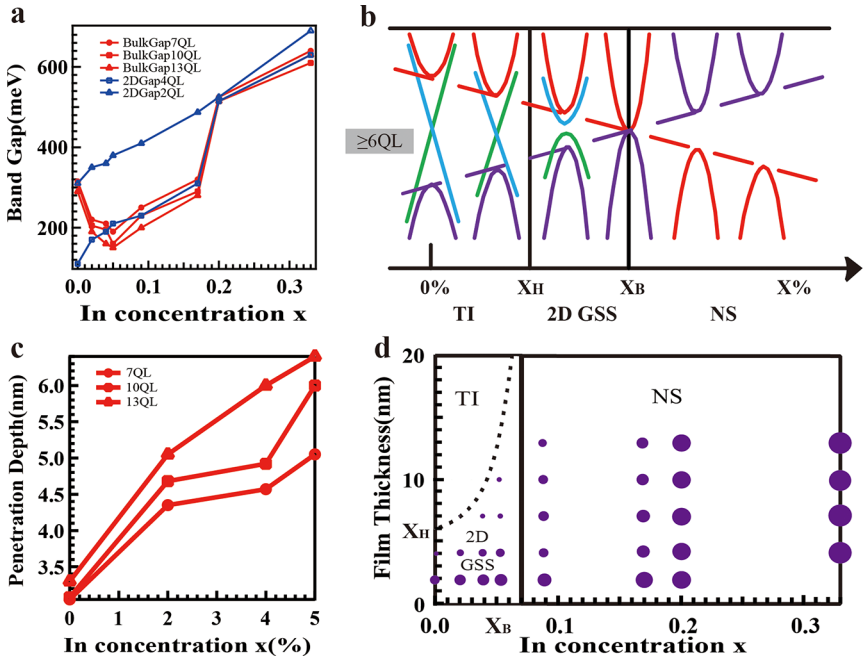

Figure 3. $(Bi_{1-x}In_x)_2Se_3$ phase evolution with various thickness and substitution. (a) Two-dimensional (in blue) and bulk (in red) gap size with various $(Bi_{1-x}In_x)_2Se_3$ In concentration for different thicknesses. (b) Schematic of band structure evolution of $(Bi_{1-x}In_x)_2Se_3$ with increasing x for films thicker than 6 QLs. (c) Surface states penetration depth with various $(Bi_{1-x}In_x)_2Se_3$ thickness and x. (d) $(Bi_{1-x}In_x)_2Se_3$ phase diagram with various film thickness and x; the solid circles represent all the data points from our ARPES results, with their size proportional to the gap size.

2a. Thus, for all the different numbers of layers, the bands of bulk and surface states can be distinguished by tracking their evolution back from the topologically nontrivial phase. In the case of $x = 0$ (Figure 2a), as reported previously,[15] coupling between the top and bottom surface state happens for Bi_2Se_3 films thinner than 6 QLs. Consequently, a surface state gap emerges. The size of this gap is estimated as 0.31 eV for 2 QLs and 0.11 eV for 4 QLs. When the thickness $\geq$ 7 QLs, the surface states are gapless, confirmed by the well-defined Dirac cone structure for 7, 10, and 13 QLs. By using a hybrid exchange-correlation functional, our DFT-calculated electronic structures of Bi_2Se_3 films show excellent agreement with the ARPES results, especially for the band gap values (see Figure 2d). Note that theoretically there is always a small gap at the Γ point due to the hybridization between the two surfaces, despite the fact that the gap is too tiny and thus can be ignored within the experimental resolution. These results agree with previous works[15,19] that, with decreasing layer number, a dimensional crossover from 3D TI to 2D GSS occurs at about 6 QLs in $(Bi_{1-x}In_x)_2Se_3$ for $x = 0$. In Figure S3 we use the second curvature method[30] to treat the ARPES spectra. With such a treatment the surface dispersion and gap are clearly distinguished, clearly proving the existence of gapped surface states.

With increasing In substitution x, the critical layer number corresponding to gapped−gapless surface states crossover also increases. For $x = 0.02$ (Figures S1a and S3b), the surface state gap increases to 0.35 and 0.17 eV for 2 and 4 QLs, respectively. Moreover, a small gap about 0.03 eV opens for 7 QLs, while 10 and 13 QLs remain gapless. For $x = 0.04$ (Figures S1b and S3c), the gap size further increases to 0.36, 0.19, and 0.05 eV for 2, 4, and 7 QLs. With x increased to 0.05 (Figure 2b and Figure S3d), another surface gap of 0.05 eV opens for 10 QLs, accompanied by the continued increase of gap size for the thinner ones. This helps us to roughly locate the 3D TI−2D GSS crossover point for $x = 0.02$ around 8 QLs, for $x = 0.04$ around 9 QLs, and for $x = 0.05$ around 12 QLs. The DFT-calculated band structures of $(Bi_{1-x}In_x)_2Se_3$ films with $x = 0.05$ are also in agreement with those obtained from ARPES. We note that there is a discrepancy between our calculation and experimental data for thick films at $x = 0.09$, which may be attributed to the experimental nonuniform substitution of In in these samples.

The increase of dimensional crossover layer number and surface gap size with substitution level x can be qualitatively explained by the surface states penetration equation: $\lambda = h\upsilon_F/2\pi E_g$,[31] in which υ_F is surface states Fermi velocity, and E_g is the bulk gap. Taking 6 QLs Bi_2Se_3 (E_g = 0.32 eV) as a reference, its penetration depth is approximate 3 nm. From the ARPES results, $(Bi_{0.98}In_{0.02})_2Se_3$ bulk gaps are estimated as 220, 205, and 190 meV for 7, 10, and 13 QLs, respectively. According to the formula above, the surface states penetration depth can be estimated as 4.35, 4.68, and 5.05 nm, respectively. For 7 QLs $(Bi_{0.98}In_{0.02})_2Se_3$ film, $2\lambda > 7$ nm. Consequently, coupling between the top and bottom surface state happens, and a narrow surface states gap emerges. For 10 and 13 QLs $(Bi_{0.98}In_{0.02})_2Se_3$ films, $2\lambda < 10$ and 13 nm, so there exists still a gapless Dirac cone. For $x = 0.05$, the bulk gaps decrease to 190, 160, and 150 meV, corresponding to a surface penetration depth of about 5.05, 6, and 6.4 nm, for 7, 10, and 13 QLs, respectively. Thus, $(Bi_{0.95}In_{0.05})_2Se_3$ 7 and 10 QLs are gapped while 13 QLs are gapless.

Phase Diagram. To approach the $(Bi_{1-x}In_x)_2Se_3$ bulk TPT point, we increase x to 9%, 17%, 20%, and 33% (Figure 2 and Figure S1). From the band structure shown for these substitution levels, no signature of Dirac cone nor surface states can be seen. We attribute the absence of the surface states to the TPT-resulted trivial topology in these films. This judgment is supported by the fact that the bulk gap size decreases with In substitution x for $x \leq 0.05$ but increases with

DOI: 10.1021/acs.nanolett.9b01641
Nano Lett. 2019, 19, 4627−4633

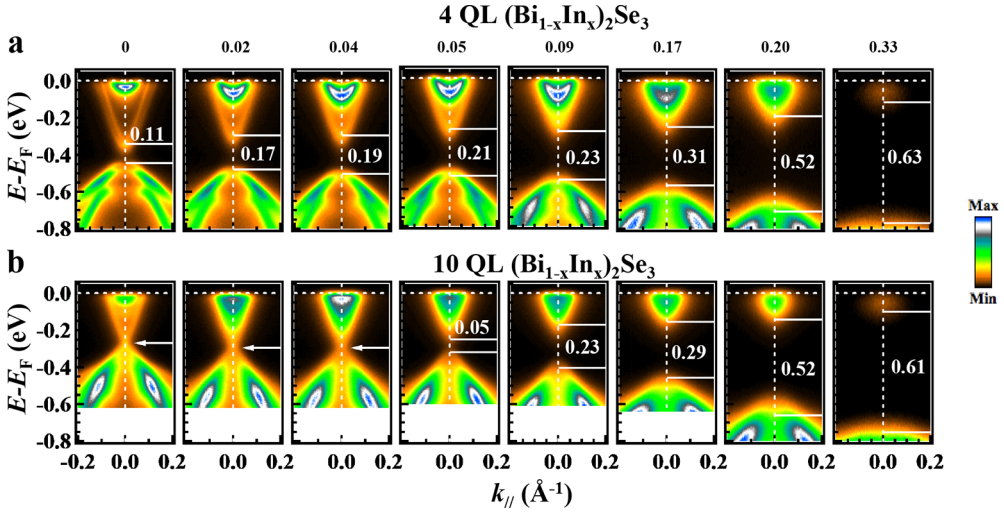

Figure 4. Band structure evolution of $(Bi_{1-x}In_x)_2Se_3$ thin films for 4 and 10 QLs with increasing substitution level x. The white solid lines indicate the VBM and CBM positions. The corresponding estimated gap size (in eV) is also shown for each composition. The white arrows indicate the position of the Dirac point.

x for $x \geq 0.09$, suggesting an inverted gap-closure and reopening process (see Figure 3a). We thus conclude that $(Bi_{1-x}In_x)_2Se_3$ films ($x > 9\%$) are in the NI phase. Furthermore, for $x < 0.33$, the Fermi level lies in the bulk conduction band for all of the thicknesses. When $x = 0.33$ (see Figure 4), the bulk conduction band is almost invisible, with only a faint tail left, in agreement with the characteristic spectra reported as a variable range-hopping insulator.[22]

In a topological nontrivial area, with the increasing of x, the bulk gap decreases gradually, as summarized in Figure 3a,b, in contrast to the sudden gap-closure scenario observed in bulk crystals.[24] Correspondingly, the surface states penetration depth increases (Figure 3c). Once the penetration depth is larger than half of the film thickness, the top and bottom surface states begin to hybridize, leading to the gap opening in the surface states. The size of this hybridization-induced surface gap increases with substitution x, also summarized in Figure 3a. The crossover from 3D TI to 2D GSS ($x = x_H$) is thickness-dependent. When the film is thicker, the x_H is larger. When x is close to the bulk critical point (x_B), the bulk gap vanishes, resulting in an infinite surface penetration depth. In this case, the $(Bi_{1-x}In_x)_2Se_3$ film will open a surface state gap regardless of the thickness, which is exactly what happens in previous works.[21−24] At x_B, the transition from 2D GSS to NI happens, independent of the number of layers. We note here that, because of the quantum well states in thin $(Bi_{1-x}In_x)_2Se_3$ films, the negative bulk gap may not close at the bulk critical point.[19]

Figure 3d demonstrates a phase diagram with the variable of x and film thickness concluded from our ARPES results. From this diagram, as indicated by the black dashed line, the dimensional crossover from 3D TI to 2D GSS state ($x = x_H$) is thickness-dependent and approaches the bulk limit x_B asymptotically. This naturally provides an experimental way to tune the dimensional crossover in $(Bi_{1-x}In_x)_2Se_3$ films by band gap engineering through thickness and substitution control. This phase evolution manipulation, together with the ability to grow atomically flat ultrathin films also proved in this work, would pave the route for the exploration of novel 2D topological states and potential device applications.

Topological Nature of Thin Films. Our ARPES results not only show the bulk TPT and the dimensional crossover of $(Bi_{1-x}In_x)_2Se_3$ films (see Figure 3) but also reveal the topological feature of Bi_2Se_3 thin films as 2D GSS systems. In principle, we can create a dynamical evolution process and see if TPT happens during the process by introducing an external knob, such as the strength of SOC, electric field, or strain. By tuning the knob, we turn the initial state with unknown topological features to a known final state, say, an NI state. If the initial state is topologically nontrivial, we would expect that the band gap decreases to zero and reopens during the evolution; otherwise the initial state is topologically trivial. Here, we consider such In substitution as an external knob that mainly modulates the strength of SOC of the system, while the lattice constant also decreases with doping. Figures 3a and 4a show the gap evolution for the case of 4 QLs as a function of In concentration x. The band gaps exhibit a monotonic increasing trend upon doping until $x = 0.20$, far beyond the bulk critical point x_B, indicating that 4 QLs Bi_2Se_3 is a 2D NI rather than 2D quantum spin Hall insulator. Theoretically, Z_2 invariant of Bi_2Se_3 QLs can be computed by the Fu-Kane formula,[32] which counts the product of the parities of all occupied states and all time-reversal-invariant momenta (TRIM). Our DFT calculations show that the thin films Bi_2Se_3 with an observable hybridization gap (i.e., 1−5 QLs) are all topologically trivial, in contrast to the previously reported oscillatory behavior between NI and TI from 3 QLs.[16,17]

As shown in Figures 4b and 3a, for 10 QLs, the gap evolution has a similar trend compared with those of 4 QLs for $x \geq 0.05$. On the other hand, although theoretically there is always a gap at the Dirac cone due to the hybridization between the opposite surfaces in a thick film, the initial states of 7 and 10 QLs films show "gapless" surface dispersion seen by ARPES as the thickness being larger than the twice the surface penetration depth. Consequently, for films thicker than 6 QLs, a dimensional crossover in the topological nontrivial phase occurs before the TPT happens at x_B. Therefore, it is not quite meaningful to treat these thick films as 2D gapped states and judge if the tiny gap is inverted or not.

In conclusion, our work represents a systematic study of a classic 3D TI system in its ultrathin form with precise thickness

DOI: 10.1021/acs.nanolett.9b01641
Nano Lett. 2019, 19, 4627−4633

and substitution control. The ARPES spectra clearly describe how the electronic structure evolves when both SOC and surface state hybridization come into play, making an essential step toward controlling the topological phase evolution for fundamental research, material engineering, and device fabrication. The combining ARPES and DFT band gap evolution analysis also demonstrates a practical solution to determine the topology of one particular phase through its phase evolution to another phase with known topology.

Methods. *Sample Preparation.* We use SiC epitaxy 1−2 layers graphene as the substrate for $(Bi_{1-x}In_x)_2Se_3$. The SiC substrates were first degassed by heating to 600 °C for 2 h in the MBE chamber until the system returns to the base pressure. Then, we heat SiC to 900 °C to remove the surface oxides. During this period, Si is evaporated to decrease the loss speed of Si in SiC. At last, a flat single layer graphene was formed by heating SiC substrates to 1300 °C for 10 min. The Bi, Se, and In sources were thermally evaporated from Knudsen cells at the same time with Bi and Se fixed on 420 and 130 °C. In concentration x was controlled by changing In evaporating temperature. The graphene substrate was kept at 200 °C while growing.

Density Functional Theory. We first calculate the electronic structures of bulk $(Bi_{1-x}In_x)_2Se_3$ alloys by first-principles calculations using the projector-augmented wave (PAW) pseudopotentials,[33] as implemented in the Vienna Simulation Package (VASP).[34] For the exchange-correlation energy, we used the screened hybrid density functional of the Heyd−Scuseria−Ernzerhof type (HSE06).[35] A 6 × 6 × 6 K-mesh is selected for the sampling of the Brillouin zone. The energy cutoff is set to 400 eV, while the total energy minimization is performed with a tolerance of 10^{-6} eV. The ions are relaxed until the atomic force is less than 10^{-3}eV/Å with fixed lattice constants a = 4.13 Å and c = 28.58 Å which are consistent with the previously reported value.[28] Spin−orbit coupling is included throughout the calculations self-consistently. We simulate the composition alloying effects by using the virtual crystal approximation (VCA) method,[36] which considers a crystal composed of fictitious "virtual" atoms that interpolate between the behavior of the atoms in the parent compounds. In our case, the potential of $(Bi_{1-x}In_x)_2Se_3$ alloy is generated by compositionally averaging the pseudopotentials of Bi and In, i.e., $V_x = xV_{In} + (1 - x)V_{Bi}$. We constructed Wannier representations by projecting the Bloch states from the first-principles calculations of bulk materials onto the p orbitals of the cations and anions. The band structures of the slabs with different quintuple layers are calculated in the tight-binding models constructed by these Wannier representations,[37−39] as implemented in the WannierTools package.[40]

■ ASSOCIATED CONTENT

Supporting Information

Supporting Information is available free of charge. The Supporting Information is available free of charge on the ACS Publications website at DOI: 10.1021/acs.nanolett.9b01641.

Band structure evolution, band structure spectra, and band structures (PDF)

■ AUTHOR INFORMATION

Corresponding Authors

*E-mail: oscarwang2008@sina.com.

*E-mail: liuqh@sustech.edu.cn.

*E-mail: chency@sustech.edu.cn.

ORCID

Zhenyu Wang: 0000-0001-6042-0873

Tian Jiang: 0000-0003-3343-5548

Author Contributions

Z.W., T.Z., and T.J. contributed equally to this paper. The manuscript was written through contributions of all authors. All authors have given approval to the final version of the manuscript.

Notes

The authors declare no competing financial interest.

■ ACKNOWLEDGMENTS

We thank Prof. Hai-Zhou Lu for helpful discussions. This work was supported by the General Program of Beijing Academy of Quantum Information Sciences (Project Y18G17), the Opening Foundation of State Key Laboratory of High Performance Computing (201601-02), and Science, Technology and Innovation Commission of Shenzhen Municipality (ZDSYS20170303165926217, JCYJ20170412152620376).

■ REFERENCES

(1) Qi, X.-L.; Zhang, S.-C. Topological insulators and superconductors. *Rev. Mod. Phys.* **2011**, *83*, 1057−1110.

(2) Hasan, M. Z.; Kane, C. L. Colloquium: Topological insulators. *Rev. Mod. Phys.* **2010**, *82*, 3045.

(3) Ando, Y.; Fu, L. Topological Crystalline Insulators and Topological Superconductors: From Concepts to Materials. *Annu. Rev. Condens. Matter Phys.* **2015**, *6*, 361−381.

(4) Fu, L.; Kane, C. L.; Mele, E. J. Topological insulators in three dimensions. *Phys. Rev. Lett.* **2007**, *98* (10), 106803.

(5) Zhang, H.; Liu, C. X.; Qi, X. L.; Dai, X.; Fang, Z.; Zhang, S. C. Topological insulators in Bi_2Se_3, Bi_2Te_3, and Sb_2Te_3 with a single Dirac cone on the surface. *Nat. Phys.* **2009**, *5* (6), 438−442.

(6) Xia, Y.; Qian, D.; Hsieh, D.; Wray, L.; Pal, A.; Lin, H. Observation of a large-gap topological-insulator class with a single Dirac cone on the surface. *Nat. Phys.* **2009**, *5* (6), 398−402.

(7) Dzero, M.; Xia, J.; Galitski, V.; Coleman. Topological Kondo Insulators. *Annu. Rev. Condens. Matter Phys.* **2016**, *7*, 249−280.

(8) Armitage, N. P.; Mele, E. J.; Vishwanath, A. Weyl and Dirac semimetals in three-dimensional solids. *Rev. Mod. Phys.* **2018**, *90*, 015001.

(9) Grover, T.; Sheng, D. N.; Vishwanath, A. Emergent space-time supersymmetry at the boundary of a topological phase. *Science* **2014**, *344*, 280−283.

(10) Wang, C.; Potter, A. C.; Senthil, T. Classification of interacting electronic topological insulators in three dimensions. *Science* **2014**, *343*, 629−631.

(11) Lindner, N. H.; Refael, G.; Galitski, V. Floquet topological insulator in semiconductor quantum wells. *Nat. Phys.* **2011**, *7*, 490−495.

(12) Liu, Q.; Zhang, X.; Abdalla, L. B.; Fazzio, A.; Zunger, A. Switching a Normal Insulator into a Topological Insulator via Electric Field with Application to Phosphorene. *Nano Lett.* **2015**, *15*, 1222−1228.

(13) Mellnik, A. R.; Lee, J. S.; Richardella, A.; Grab, J. L.; Mintun, P. J.; Fischer, M. H.; Manchon, A.; Kim, E.-A.; Samarth, N.; Ralph, D. C. Spin-transfer torque generated by a topological insulator. *Nature* **2014**, *511*, 449−451.

(14) Qian, X.; Fu, L.; Li, J. Topological crystalline insulator nanomembrane with strain-tunable band gap. *Nano Res.* **2015**, *8*, 967−979.

(15) Zhang, Y.; He, K.; Chang, C. Z.; Song, C. L.; Wang, L. L.; Chen, X.; Jia, J. F.; Fang, Z.; Dai, X.; Shan, W. Y.; Shen, S. Q.; Niu, Q.; Qi, X. L.; Zhang, S. C.; Ma, X. C.; Xue, Q. K. Crossover of the

DOI: 10.1021/acs.nanolett.9b01641
Nano Lett. 2019, 19, 4627−4633

three-dimensional topological insulator Bi_2Se_3 to the two-dimensional limit. *Nat. Phys.* **2010**, *6*, 584−588.
(16) Lu, H.-Z.; Shan, W.-Y.; Yao, W.; Niu, Q.; Shen, S.-Q. Massive Dirac fermions and spin physics in an ultrathin film of topological insulator. *Phys. Rev. B: Condens. Matter Mater. Phys.* **2010**, *81*, 115407.
(17) Liu, C.-X.; Zhang, H. J.; Yan, B. H.; Qi, X. L.; Frauenheim, T.; Dai, X.; Fang, Z.; Zhang, S. C. Oscillatory crossover from two-dimensional to three-dimensional topological insulators. *Phys. Rev. B: Condens. Matter Mater. Phys.* **2010**, *81*, 041307.
(18) Park, B. C.; Kim, T. H.; Sim, K. I.; Kang, B. K.; Kim, J. W.; Cho, B.; Jeong, K.-H.; Cho, M.-H.; Kim, J. H. Terahertz single conductance quantum and topological phase transitions in topological insulator Bi_2Se_3 ultrathin films. *Nat. Commun.* **2015**, *6*, 6552.
(19) Salehi, M.; Shapourian, H.; Koirala, N.; Brahlek, M. J.; Moon, J.; Oh, S. Finite-Size and Composition-Driven Topological Phase Transition in $(Bi_{1-x}In_x)_2Se_3$ Thin Films. *Nano Lett.* **2016**, *16*, 5528−5532.
(20) Xu, S. Y.; Xia, Y.; Wray, L. A.; Jia, S.; Meier, F.; Dil, J. H.; Osterwalder, J.; Slomski, B.; Bansil, A.; Lin, H.; Cava, R. J.; Hasan, M. Z. Topological phase transition and Texture Inversion in a Tunable Topological Insulator. *Science* **2011**, *332*, 560.
(21) Sato, T.; Segawa, K.; Kosaka, K.; Souma, S.; Nakayama, K.; Eto, K.; Minami, T.; Ando, Y.; Takahashi, T. Unexpected mass acquisition of Dirac fermions at the quantum phase transition of a topological insulator. *Nat. Phys.* **2011**, *7*, 840−844.
(22) Brahlek, M.; Bansal, N.; Koirala, N.; Xu, S. Y.; Neupane, M.; Liu, C.; Hasan, M. Z.; Oh, S. Topological-metal to band-insulator transition in $(Bi_{1-x}In_x)_2Se_3$ thin films. *Phys. Rev. Lett.* **2012**, *109*, 186403.
(23) Wu, L.; Brahlek, M.; Aguilar, R. V.; Stier, A. V.; Morris, C. M.; Lubashevsky, Y.; Bilbro, L. S.; Bansal, N.; Oh, S.; Armitage, N. P. A sudden collapse in the transport lifetime across the topological phase transition in $(Bi_{1-x}In_x)_2Se_3$. *Nat. Phys.* **2013**, *9*, 410−414.
(24) Lou, R.; Liu, Z. H.; Jin, W. C.; Wang, H. F.; Han, Z. H.; Liu, K.; Wang, X. Y.; Qian, T.; Kushnirenko, Y.; Cheong, S. W.; Osgood, R. M.; Ding, H.; Wang, S. Sudden gap closure across the topological phase transition in $Bi_{2-x}In_xSe_3$. *Phys. Rev. B: Condens. Matter Mater. Phys.* **2015**, *92*, 115150.
(25) Zhang, C.; Yuan, X.; Wang, K.; Chen, Z. G.; Cao, B. B.; Wang, W. Y.; Liu, Y. W.; Zou, J.; Xiu, F. X. Observations of a Metal-Insulator Transition and Strong Surface States in $Bi_{2-x}Sb_xSe_3$ Thin Films. *Adv. Mater.* **2014**, *26*, 7110−7115.
(26) Dziawa, P.; Kowalski, B. J.; Dybko, K.; Buczko, R.; Szczerbakow, A.; Szot, M.; Łusakowska, E.; Balasubramanian, T.; Wojek, B. M.; Berntsen, M. H.; Tjernberg, O.; Story, T. Topological crystalline insulator states in $Pb_{(1-x)}Sn_{(x)}Se$. *Nat. Mater.* **2012**, *11*, 1023−1027.
(27) Song, C. L.; Wang, Y. L.; Jiang, Y. P.; Zhang, Y.; Chang, C. Z.; Wang, L. L.; He, K.; Chen, X.; Jia, J. F.; Wang, Y. Y.; Fang, Z.; Dai, X.; Xie, X. C.; Qi, X. L.; Zhang, S. C.; Xue, Q. K.; Ma, X. C. Topological insulator Bi_2Se_3 thin films grown on double-layer graphene by molecular beam epitaxy. *Appl. Phys. Lett.* **2010**, *97*, 143118.
(28) Wang, Z. Y.; Guo, X.; Li, H. D.; Wong, T. L.; Wang, N.; Xie, M. H. Superlattices of Bi_2Se_3/In_2Se_3: growth characteristics and structural properties. *Appl. Phys. Lett.* **2011**, *99*, 023112.
(29) Zhang, G. H.; Qin, H. J.; Teng, J.; Guo, J. D.; Guo, Q. L.; Dai, X.; Fang, Z.; Wu, K. H. Quintuple-layer epitaxy of thin films of topological insulator Bi_2Se_3. *Appl. Phys. Lett.* **2009**, *95*, 053114.
(30) Zhang, P.; Richard, P.; Qian, T.; Xu, Y. M.; Dai, X.; Ding, H. A precise method for visualizing dispersive features in image plots. *Rev. Sci. Instrum.* **2011**, *82*, 043712.
(31) Linder, J.; Yokoyama, T.; Sudbo, A. Anomalous finite size effects on surface states in the topological insulator Bi_2Se_3. *Phys. Rev. B: Condens. Matter Mater. Phys.* **2009**, *80*, 205401.
(32) Fu, L.; Kane, C. L. Topological insulators with inversion symmetry. *Phys. Rev. B: Condens. Matter Mater. Phys.* **2007**, *76*, 045302.
(33) Kresse, G.; Joubert, D. From ultrasoft pseudopotentials to the projector augmented-wave method. *Phys. Rev. B: Condens. Matter Mater. Phys.* **1999**, *59*, 1758.
(34) Kresse, G.; Furthmüller, J. Efficient iterative schemes for ab initio total-energy calculations using a plane-wave basis set. *Phys. Rev. B: Condens. Matter Mater. Phys.* **1996**, *54*, 11169.
(35) Krukau, A. V.; Vydrov, O. A.; Izmaylov, A. F.; Scuseria, G. E. Influence of the exchange screening parameter on the performance of screened hybrid functionals. *J. Chem. Phys.* **2006**, *125*, 224106.
(36) Yu, C. J.; Emmerich, H. An efficient virtual crystal approximation that can be used to treat heterovalent atoms, applied to $(1-x)BiScO_{3-x}PbTiO_3$. *J. Phys.: Condens. Matter* **2007**, *19*, 306203.
(37) Marzari, N.; Vanderbilt, D. Maximally Localized Generalized Wannier Functions for Composite Energy Bands. *Phys. Rev. B: Condens. Matter Mater. Phys.* **1997**, *56*, 12847.
(38) Souza, I.; Marzari, N.; Vanderbilt, D. Maximally Localized Wannier Functions for Entangled Energy Bands. *Phys. Rev. B: Condens. Matter Mater. Phys.* **2001**, *65*, 035109.
(39) Mostofi, A. A.; Yates, J. R.; Pizzi, G.; Lee, Y. S.; Souza, I.; Vanderbilt, D.; Marzari, N. An Updated Version ofWANNIER90: A Tool for Obtaining Maximally-Localised Wannier Functions. *Comput. Phys. Commun.* **2014**, *185*, 2309.
(40) Wu, Q. S.; Zhang, S. N.; Song, H. F.; Troyer, M.; Soluyanov, A. A. WannierTools: An open-source software package for novel topological materials. *Comput. Phys. Commun.* **2018**, *224*, 405.

DOI: 10.1021/acs.nanolett.9b01641
Nano Lett. 2019, 19, 4627−4633